WATER TRANSPORT IN THE MARTIAN NORTHERN WINTER POLAR ATMOSPHERE

D. J. McCleese, *Synoptic Science, Altadena, CA,* **H. E. Gillespie,** *Lunar and Planetary Institute, Houston, TX (hgillespie@lpi.usra.edu),* **A. Kleinböhl, D. M. Kass,** *Jet Propulsion Laboratory, California Institute of Technology, Pasadena, CA,* **S. J. Greybush,** *Pennsylvania State University, University Park, PA,* **R. J. Wilson,** *Ames Research Center, Mountain View, CA*

Introduction:

The Martian polar vortices are challenging to study in part due to the large gradients in temperature, wind, and aerosol fields at their boundaries as well as the transient and stationary waves that often have their largest amplitudes near the polar vortex boundaries. This work focuses on water transport in the vicinity of, and particularly at the boundary of, the northern winter polar vortex in Mars Year (MY) 30, as observed by the Mars Climate Sounder (MCS) [1] and simulated by the Ensemble Mars Atmosphere Reanalysis System (EMARS) [2]. Understanding of cross-boundary transport is crucial to understanding the Martian water cycle, particularly the influence of the multiple kilometers thick permanent north polar water ice cap. During the northern winter, water from most of Mars is transported by the Hadley circulation to the winter pole, where it is deposited onto the north polar ice cap. Several prior studies have investigated transport across the polar vortex boundary, including for varying obliquity over Martian climate cycles [3] and using the "age-of-air" diagnostic [4]. Here, we investigate transport across a dynamic polar vortex boundary as a function of altitude, longitude, and Ls.

Datasets:

MCS is an infrared radiometer aboard the Mars Reconnaissance Orbiter. MCS observes the atmosphere of Mars at approximately 3 AM and 3 PM local time and has observed the atmosphere of Mars since MY 28. Vertical profiles of temperature, dust opacity, and water ice opacity are retrieved from MCS radiances [5], and extend from the surface to about 80 km above the surface, with a vertical resolution of about 5 km.

EMARS is a reanalysis that combines the Geophysical Fluid Dynamics Laboratory Mars Global Climate Model (MGCM) with MCS observations using data assimilation, specifically the local ensemble transform Kalman filter (LETKF) [6]. Data assimilation enables EMARS to have full coverage in longitude, latitude, altitude, and time of any variables of interest in the Martian atmosphere, as models do, while retaining information about Martian weather from observations. EMARS assimilates vertical profiles of temperature from MCS, and the assimilation updates temperature, horizontal wind, and surface pressure. Dust is prescribed in the lowest model levels to conform to column dust opacities in [7], representing lifting and sedimentation of dust in the boundary layer. The grid spacing of EMARS is 5° latitude x 6° longitude, with 28 vertical levels extending from the surface to about 100 km above the surface on hybrid σ-p surfaces. The EMARS control run, hereafter called the "free run," is a run of EMARS without data assimilation. A comparison of EMARS with its free run allows us to determine the effects of assimilation on the modeled Martian atmosphere, and comparison with MCS when possible enables us to assess how close EMARS is to the true state of the Martian atmosphere.

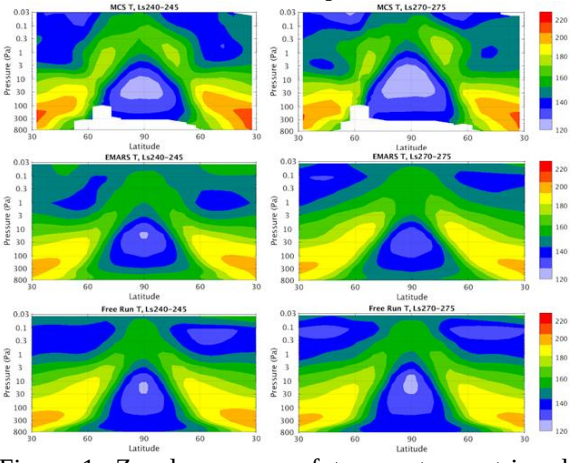

Figure 1. Zonal averages of temperature retrieved from MCS measurements (top) compared with EMARS (middle) and the free run (bottom). The left three panels are Ls 240°-245°; right three panels are Ls 270°-275°.

Behavior of the Polar Vortex:

We begin our analysis of the northern winter polar vortex in MY 30 by examining zonal mean temperature, dust, and water ice over the pole in MCS, EMARS, and the free run (Figure 1). In Figure 1, the left side of each panel shows values at 3 AM local time, while the right side shows values at 3 PM local time. The vortex is only shown here for 5 Ls intervals following Ls 240 and Ls 270, but qualitatively, the fields shown in Figure 1 persist from Ls 225 to Ls 315 with little change. In all cases, the maximum temperatures in the midlatitudes increase in altitude (decrease in pressure) from about 300 Pa at 30 N to about 30 Pa at 60 N. In the polar region, the maxi-

mum temperature increases in altitude more rapidly when approaching the pole, with the maximum in temperature at about 0.3 Pa over the pole. EMARS improves the slope of the maximum thermal gradient between the polar vortex and the midlatitudes, whereas the free run vortex is tall and narrow, comparatively. The horizontal temperature gradient is key to understanding the polar vortex boundary on its own as well as through its connection to thermal wind balance and potential vorticity. Temperatures are generally improved in EMARS compared to the free run, with the notable exception of the interior of the polar vortex at Ls 270.

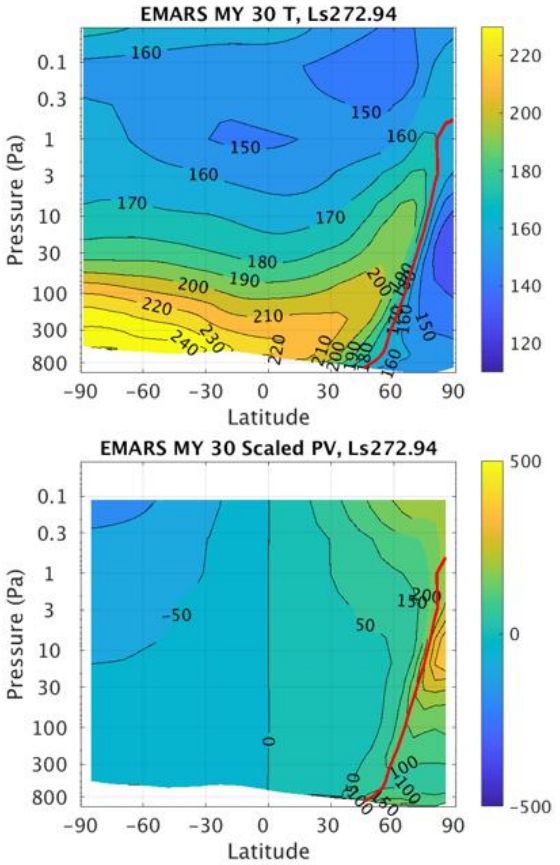

Figure 2. The upper panel is zonal mean temperature from EMARS with the vortex boundary bolded red; the lower panel is the scaled potential vorticity following [8]. The units for the lower panel are scaled PVU (10^{-6}m^{2}s^{-1}kg^{-1}K).

In order to assess transport in and out of the polar vortex, we must adopt a definition of the polar vortex boundary. The polar vortex boundary has been defined in a variety of ways, including the maximum meridional potential vorticity gradient and the maximum meridional temperature gradient. Here, we choose a simple, observable definition that roughly coincides with previous definitions of the polar vortex for Mars, as shown in Figure 2: the 170 K isotherm, with a few modifications. Note that scaled potential vorticity, defined following [8], reduces the vertical gradient of potential vorticity without affecting the horizontal gradient of potential vorticity substantially. None of the definitions of the polar vortex work well near the surface, so we assume that the lowest 1 km of the vortex has a vertical boundary. Specifically, a grid cell of EMARS or the free run is in the vortex if these 5 conditions apply:

1) Its temperature is below 170 K

2) No cell closer to the north pole at the same longitude, height, and time is above 170 K in temperature

3) A cell further from the north pole is above 170 K in temperature

4) It is not on the topmost two model levels

5) It is below 1 km altitude and the cell directly above it at 1 km is in the vortex.

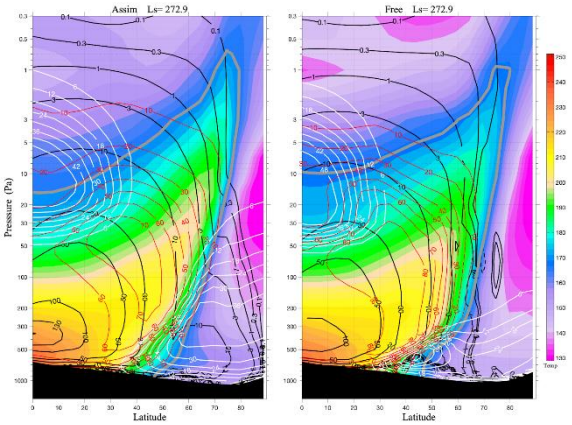

Figure 3. Zonal mean streamfunction, and other quantities, in the free run (left) and reanalysis (right) averaged over 5 sols after winter solstice. Streamfunction (10^8 kg/s) is in black, water vapor mass mixing ratio (10^{-6} kg/kg) is in red, water ice mass mixing ratio (also ppm) is in white, and temperature is in color. The 170 K contour is marked in bold gray.

Water Transport in the Northern Winter Polar Vortex:

Water transport near the northern polar vortex differs substantially between EMARS and its free run. In particular, substantially more water enters the polar vortex in EMARS than in the free run. Figure 3, in particular the zonal mean streamfunction, is indicative of this increase in transport. In the free run, lines of constant streamfunction do not cross the polar vortex boundary above 100 Pa, and substantial cross-boundary transport occurs only below 300 Pa. Lines of constant streamfunction are approximately parallel to the vortex edge at high altitude, suggesting little to no transport of any quantity into the polar vortex at high altitude in the free run. However, the EMARS streamfunction shows substantial cross-boundary transport up to at least 10 Pa, with lines of constant streamfunction bending into the polar vortex at the vortex boundary. Compounding this difference in the winds, as inferred by the streamfunction, is the increased availability of water vapor and water ice at the vortex edge in EMARS above 500 Pa. A temperature increase of about 10 K near the surface

within and just outside the polar vortex in EMARS compared to the free run are consistent with adiabatic warming produced by an enhanced, cross-boundary Hadley circulation. It seems that the increased cross-boundary transport causes vertically extended water ice clouds to appear within the EMARS vortex, which has been a challenging feature of MCS observations to reproduce with Mars models [9]. This cross-boundary transport in EMARS persists not only through nearly the entirety of the northern winter, but also does not vary substantially among Martian years lacking a global dust storm.

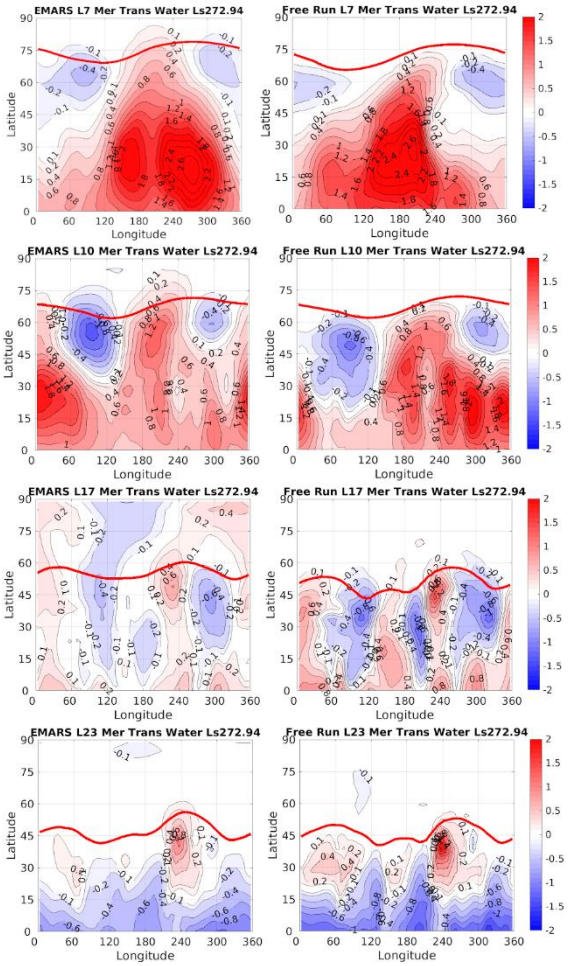

Figure 4. EMARS (left) and free run (right) simulated cross-sections of mean water transport at four model levels L7 (10 Pa, 45 km), L10 (36 Pa, 30 km), L17 (300 Pa, 7 km) and L23 (550 Pa, 1 km) above the surface for Ls 270° to 275° in MY 30. The units of meridional transport of water are (m/s)*(kg water/kg air)*10^3.

Figure 4 shows latitude-longitude cross-sections of mean water (vapor and ice) transport at four model levels in the atmosphere. This figure enables us to see variation in transport with longitude not visible in the zonal mean. Notice that transport, as well as the vortex boundary, are dominated by a wavenumber 1 stationary wave in the upper atmosphere that transitions to wavenumber 2 in the lower atmosphere. Near-surface transport may result primarily from katabatic winds from Alba Patera (41°N, 249°E). Also observe that in the free run, water transport tends to stop at the polar vortex boundary, while in EMARS, transport continues across the boundary unimpeded.

Figure 5 explores the vertical dimension of the total water transport as a time mean across the dynamic vortex boundary between Ls 270 and Ls 300. In the free run, water is primarily transported into the vortex at altitudes below the 200 Pa surface. Transport into the vortex is dominated by vertical transport, and horizontal transport acts partially in opposition to the vertical transport, removing some of the water added to the vortex. The variability of vertical transport in the free run may be due to the greater surface area of the vortex at lower altitudes than 200 Pa compared to high altitudes. In EMARS, the maximum water transport occurs between 50 and 100 Pa, and comparatively less transport into the vortex occurs between 200 and 450 Pa, where the free run transport into the vortex is greatest. The vertical transport into the vortex is approximately constant with height, suggesting a vortex edge that is approximately uniformly sloping with height, as seen in Figure 4. Variations in transport with height in EMARS are primarily horizontal. In total, we find that between Ls 240 and 300, in EMARS, transport into the vortex is about 6 Tg/sol, with about 2 Tg/sol occurring at altitudes below the 200 Pa surface. In the free run, transport into the vortex is less than 4 Tg/sol, and nearly all of it occurs below 200 Pa.

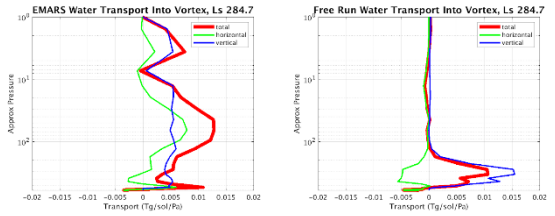

Figure 5. Water transport into the polar vortex in the EMARS (left) and the free run (right) as a function of height, in Tg/sol/Pa, averaged from Ls 270 to Ls 300. Total transport is shown in bold red, the transport due to the horizontal wind is shown in green, and the transport due to vertical wind is shown in blue.

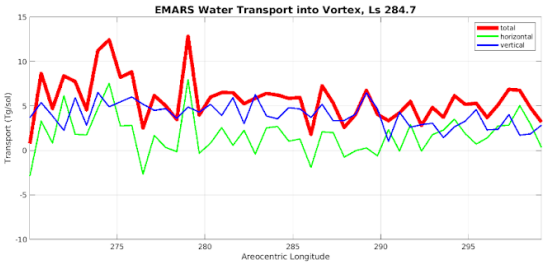

Figure 6. Water transport into the polar vortex in EMARS during Ls 270°-300°. Total transport is

shown in bold red, which is split into the amount of transport into the vortex parallel to isentropes (green) and perpendicular to the isentropes (blue).

Figure 6 shows the total transport across the vortex boundary, divided into components parallel and perpendicular to isentropes. This decomposition assists us in understanding why water is transported across the vortex boundary. Transport parallel to isentropes is caused by adiabatic processes (typically), and transport perpendicular to isentropes is caused by diabatic processes. In EMARS, most of the transport is cross-isentropic, which is indicative of diabatic cooling, namely radiative cooling of air in the descending branch of the Hadley circulation. A similar result holds for the free run (not shown).

Conclusions:

Our study of water transport shows that the northern polar vortex is somewhat porous to water. According to EMARS, about 6 Tg/sol water enters the polar vortex, and most of the water enters the vortex above 200 Pa as part of the global Hadley circulation. The vortex boundary and transport across it are highly variable in all spatiotemporal dimensions in EMARS. The free run captures neither the upper atmosphere transport into the vortex nor the variability of the vortex boundary and transport across it. Measurements of wind and additional measurements of water, particularly water vapor, in and around the polar vortex with sufficient spatiotemporal coverage to be included in data assimilation would be helpful in improving the representation of water transport in Mars simulations as well as in assessing water transport in the real Martian atmosphere.

Acknowledgments:

Participation by HEG and SJG in this research has been funded by NASA MDAP awards 80NSSC17K0690 and 80NSSC20K1054. EMARS and MGCM control run data are publicly available through the Penn State Data Commons, and access is described in [2]. Work at the Jet Propulsion Laboratory, California Institute of Technology, was performed under a contract with the National Aeronautics and Space Administration. The Jet Propulsion Laboratory also supported work through contract 1581456. The MCS data set is freely available from NASA's Planetary Data System (PDS): https://atmos.nmsu.edu/data_and_services/atmospheres_data/MARS/mcs.html.

References:

[1] McCleese, D. J., et al. (2007). "Mars Climate Sounder: An Investigation of Thermal and Water Vapor Structure, Dust and Condensate Distributions in the Atmosphere, and Energy Balance of the Polar Regions," J. Geophys. Res., 112, E05S06, doi:10.1029/2006JE002790

[2] Greybush, S. J., et al. (2019). The Ensemble Mars Atmosphere Reanalysis System (EMARS) Version 1.0, Geosci Data J., 6, 137-150, doi:10.1002/gdj3.77

[3] Toigo, A.D., D.W. Waugh, and S.D. Guzewich (2020), Atmospheric transport into polar regions on Mars in different orbital epochs. Icarus, 347, https://doi.org/10.1016/j.icarus.2020,113816

[4] Waugh, D.W., A.D. Toigo, and S.D. Guzewich (2018), Age of Martian air: Time scales for Martian atmospheric transport. Icarus 317, https://doi.org/10.1016/j.icarus.2018.087.002

[5] Kleinböhl, A., et al. (2009). Mars Climate Sounder limb profile retrieval of atmospheric temperature, pressure, dust and water ice opacity. J. Geophys. Res., 114, E10006, doi:10.1029/2009JE003358

[6] Hunt, B. R., E. J. Kostelich, and I. Szunyogh (2007), Efficient data assimilation for spatiotemporal chaos: A local ensemble transform Kalman filter, Physica D, 230, 112–126, doi: 10.1016/j.physd.2006.11.008

[7] Montabone, L., F. Forget, E. Millour, R.J. Wilson, S.R. Lewis, B. Cantor, D. Kass, A. Kleinböhl, M.T. Lemmon, M.D. Smith, M.J Wolff (2015). Eight-year climatology of dust optical depth on Mars, Icarus, 251, 65-95.

[8] Waugh, D. W., A. D. Toigo, S. D. Guzewich, S. J. Greybush, R. J. Wilson, and L. Montabone (2016), Martian polar vortices: Comparison of reanalyses, J. Geophys. Res. Planets, 121, 1770–1785, doi:10.1002/2016JE005093

[9] Haberle, R.M, M. Kahre, J.L. Hollingsworth, F. Montmessin, R.J. Wilson, et al., (2019), Documentation of the NASA/Ames Mars Global Climate Model: Simulations of the present seasonal water cycle. Icarus, https://doi.org/10.1016/j.icarus.2019.03.026